J. Biomechanics Vol. 24, No. 7, pp. 527–538, 1991.
Printed in Great Britain

0021-9290/91 $3.00 + .00
Pergamon Press plc

A TWO-PHASE FINITE ELEMENT MODEL OF THE DIASTOLIC LEFT VENTRICLE

JACQUES M. HUYGHE,*‡ DICK H. VAN CAMPEN,‡ THEO ARTS* and ROBERT M. HEETHAAR§

*Department of Biophysics, University of Limburg, Maastricht, The Netherlands; ‡Department of Mechanical Engineering, Eindhoven University of Technology, Eindhoven, The Netherlands and §Department of Biomedical Engineering, Twente University, Enschede, The Netherlands

Abstract—A porous medium finite element model of the passive left ventricle is presented. The model is axisymmetric and allows for finite deformation, including torsion about the axis of symmetry. An anisotropic quasi-linear viscoelastic constitutive relation is implemented in the model. The model accounts for changing fibre orientation across the myocardial wall. During passive filling, the apex rotates in a clockwise direction relative to the base for an observer looking from apex to base. Within an intraventricular pressure range of 0–3 kPa the rotation angle of all nodes remained below 0.1 rad. Diastolic viscoelasticity of myocardial tissue is shown to reduce transmural differences of preload-induced sarcomere stretch and to generate residual stresses in an unloaded ventricular wall, consistent with the observation of opening angles seen when the heart is slit open. It is shown that the ventricular model stiffens following an increase of the intracoronary blood volume. At a given left ventricular volume, left ventricular pressure increases from 1.5 to 2.0 kPa when raising the intracoronary blood volume from 9 to 14 ml (100 g)$^{-1}$ left ventricle.

NOTATION

a	scalar
$\mathbf{a}$	vector
$\underline{a}$	second order tensor
$\underline{I}$	unit second order tensor
$\det \underline{a}$	determinant of $\underline{a}$
$\mathbf{ab}$	dyadic product of the vectors $\mathbf{a}$ and $\mathbf{b}$
$\mathbf{a}\cdot\mathbf{b}$	dot product of the vectors $\mathbf{a}$ and $\mathbf{b}$
$\underline{a}\cdot\mathbf{b}$	dot product of the second order tensor $\underline{a}$ and the vector $\mathbf{b}$

NOMENCLATURE

Σ^0	relaxation parameter
d	relaxation parameter
c^c	volumetric modulus
c^n	initial normal stiffness
a^f	exponential factor in fibre stiffness
a^{cf}	exponential factor in cross-fibre stiffness
a^b	exponential factor in biaxial stiffness
c^s	initial shear stiffness
a^s	exponential factor in shear stiffness
$\mathbf{B}_i$	local orthonormal basis (Fig. 2)
$\mathbf{B}'_i$	local orthonormal basis (Fig. 4)
C	volumetric strain energy
d	relaxation parameter
F_{ij}	Green strain components in reference frame $\mathbf{B}_i$
$\underline{F}$	deformation tensor
G	reduced relaxation function
J	Jacobian ($= \det \underline{F}$)
$\underline{K}$	current permeability tensor
$\underline{K}^0$	initial permeability tensor
l^s	current sarcomere length
L^s	initial sarcomere length
n^f	current porosity
N^f	initial porosity
p	intramyocardial pressure
$\mathbf{q}$	relative fluid velocity
s	effective Cauchy stress
$\underline{s}^t$	total Cauchy stress
S_{ij}	second Piola–Kirchhoff effective stress components in reference frame $\mathbf{B}_i$
S^e_{ij}	elastic part of S_{ij} due to volume change
S^s_{ij}	viscoelastic part of S_{ij} mainly due to shape change
t	time
$\mathbf{u}$	displacement vector
W	strain energy associated with shape change
$\mathbf{x}$	current position vector of solid phase
$\mathbf{X}$	initial position vector of solid phase
τ_1	lower bound of relaxation spectrum
τ_2	upper bound of relaxation spectrum
Σ'^0	relaxation parameter
θ	Crank–Nicholson constant

Received in final form 4 *December* 1990.

†Address correspondence to: Dr J. M. Huyghe, Dept of Movement Sciences, School of Health Sciences, University of Limburg, P.O. Box 616, 6200MD Maastricht, The Netherlands. Tel: 31-43-437788; Fax: 31-43-436080; Telex: 56726.

INTRODUCTION

Heart muscle is a mixture of many different components: muscle fibres, collagen fibres, coronary vessels, coronary blood and interstitial fluid. In this article we apply a mixture theory (Bowen, 1976) to the mechanics of the left ventricular myocardium. In order to reduce the complexity of the computation we restrict ourselves to a two-component mixture: a solid component and a liquid component. Finite deformation theory of liquid–solid mixtures was first formulated by Biot (1972). This theory has been presented as a special case of the theory of mixtures by Bowen (1980). The biphasic theory has been used to analyse small deformation of articular cartilage (Mow *et al.*, 1980) and intervertebral disc (Simon *et al.*, 1985). Large deformation biphasic analyses have been dealt with by Oomens *et al.* (1987) for the skin and by Kwan *et al.* (1990) for cartilage.

The stress in the liquid component is described by an intramyocardial pressure. The stress in the solid is a

full three-dimensional stress tensor. The triaxial constitutive relation for the solid is expressed in terms of a local Cartesian coordinate frame, the orientation of which depends on the local fibre direction. In order to simulate the redistribution of coronary blood in the ventricular wall during deformation, the liquid phase is allowed to flow relative to the solid. This flow is assumed to obey Darcy's law, i.e. the flow is proportional to the local intramyocardial pressure gradient. In the present set-up the model does not account for the pressure difference between arterial coronary blood and venous coronary blood. So the model does not describe coronary blood flow in the sense of a flow from arteries to veins. It is shown that even with such crude approximation of the liquid phase, several aspects of the influence of the coronary blood volume on ventricular mechanisms can be simulated. The finite element formulation used is similar to the one presented by Oomens *et al.* (1987) for the skin and subcutis. However, the new formulation allows the use of anisotropic permeability and curvilinear coordinates. Moreover, non-linearities in the mass balance equation are corrected for.

MIXTURE THEORY

The cardiac tissue is considered to be a mixture of an incompressible solid and an incompressible fluid. The current position $\mathbf{x}$ of the solid particles averaged over a representative elementary volume (REV) depends on their average initial position $\mathbf{X}$ and time t:

$$\mathbf{x} = \mathbf{x}(\mathbf{X}, t). \tag{1}$$

The REV is considerably larger than the pore size, so that the function $\mathbf{x}(\mathbf{X}, t)$ is continuous and differentiable. The average local deformation is given by the deformation tensor:

$$\underline{F} = \frac{\partial \mathbf{x}}{\partial \mathbf{X}}. \tag{2}$$

The determinant of the deformation tensor

$$J = \det \underline{F} \tag{3}$$

represents the relative volume change of the REV. Because solid and fluid are incompressible, this volume change indicates a change in fluid content of the REV. Define the initial and current fluid fractions of the REV as N^f and n^f, respectively. Then it holds that:

$$J - 1 = n^f J - N^f. \tag{4}$$

The stress in the deformed mixture is best understood as follows. Say the solid phase is subjected to the deformation $\underline{F}$ in the absence of fluid. The stress $\underline{s}$ in the solid induced by this deformation and measured per unit bulk surface is called effective stress. The word 'effective' indicates that this part of the stress is the only part depending directly on deformation. Now we inject fluid at a pressure p into the deformed solid matrix. The pressure p will spread in both the fluid and the solid. So, the total Cauchy stress in the mixture is:

$$\underline{s}^t = \underline{s} - \underline{I}p. \tag{5}$$

Applying the principle of Terzaghi (1943), saying that the pressure p does not induce deformation, the constitutive relation of the solid is expressed as a relationship between the effective second Piola–Kirchhoff stress $\underline{S}$, Green strain tensor $\underline{E}$ and time t (see Appendix). The relative velocity averaged over a bulk volume of the deformed mixture is denoted by $\mathbf{q}$. It holds according to Darcy's law in Eulerian form:

$$\mathbf{q} = -\underline{k} \cdot \frac{\partial p}{\partial \mathbf{x}} \tag{6}$$

where the permeability tensor $\underline{k}$ appears to be symmetric (Biot, 1972). In order to ensure the invariance with respect to rigid body rotation relationship (6) is transformed to its Lagrangian form (Biot, 1972):

$$\mathbf{Q} = -\underline{K} \cdot \frac{\partial p}{\partial \mathbf{X}}. \tag{7}$$

In the quasi-static approach, conservation of momentum requires:

$$\nabla \cdot \underline{s} - \nabla p = 0. \tag{8}$$

$\mathbf{u} = \mathbf{x} - \mathbf{X}$ is the displacement of the solid. Conservation of mass requires:

$$\nabla \cdot \dot{\mathbf{u}} + \nabla \cdot \mathbf{q} = 0 \tag{9}$$

in which $\nabla \cdot \dot{\mathbf{u}}$, the divergence of the solid velocity, is the volume increase of a unit volume of mixture and $\nabla \cdot \mathbf{q}$, the divergence of the specific fluid velocity, is the fluid volume squeezed out from a unit volume of mixture. Equation (9) together with equation (4) enforce incompressibility of both fluid and solid. As equations (8) and (9) do not introduce material parameters, the requirement of invariance of the parameters with respect to rigid body rotations do not apply to these equations and a transformation to their Lagrangian form is superfluous. Equations (8) and (9) are a coupled set of equations which can be solved for the displacement field $\mathbf{u}$ and the intramyocardial pressure field p. The equations are non-linear due to the geometrical and physical non-linearities. An additional non-linearity which is introduced is a deformation-dependent permeability. When the fluid is squeezed out of the mixture, the pore size decreases and the permeability decreases along with it. Following Arts [1978, p. 83, equation (6.3.3)], we may assume a quadratic dependency of the permeability on the fluid volume:

$$\underline{K} = \left(\frac{n^f}{N^f}\right)^2 {}^0\underline{K}. \tag{10}$$

FINITE ELEMENT FORMULATION

The set of two coupled equations (8) and (9) are to be solved. The finite element program is developed

for a Lagrangian description of axisymmetric deformation of an axisymmetric left ventricle. An eight-node isoparametric element is used (Fig. 1), in which the nodes are fixed to the solid and the fluid flows through the element. Quadratic shape functions are used for geometry, transmural course of fibre direction and radial, axial and circumferential displacements. Freedom of circumferential displacement allows for torsion of the left ventricle. The shape functions for the intramyocardial pressure field are linear: the pressures at the corner nodes 1, 3, 5, 7 (Fig. 1) define the pressure field of the element. Displacements have to be calculated in all nodes. This choice of elemental structure results in a comparable accuracy for the effective stress and for the intramyocardial pressure (Meijer, 1985). There was no evidence of 'checker board effect' even at large deformations (Green strains >0.6). Quadratic interpolation of the intramyocardial pressure (eight nodal pressures per element) did cause checker boarding at large deformations and was therefore not used. Integration of the volume and surface integrals are obtained by means of 3×3 and three point Gauss-integration respectively. An implicit–explicit one-step time integration scheme is used, in which the pressure is a weighted average of the intramyocardial pressure at the beginning and at the end of the timestep:

$$p = \theta p_{n+1} + (1-\theta) p_n \tag{11}$$

in which θ is the Crank–Nicholson constant. Equation (11) is used for each nodal pressure.

GEOMETRY AND BOUNDARY CONDITIONS

We already pointed out that a viscoelastic body has no well-defined stress-free state. Nevertheless, the finite element analysis needs to start at some chosen state which is assumed to be stress-free. The geometry of the left ventricle in this reference state is derived from 11 cross-sections of a canine diastolic heart obtained by means of multiplanar X-ray tomography and supplied by the Biodynamics group of the Mayo clinic, Rochester, Minnesota. Although we are aware that a diastolic heart is generally not stress-free, the diastolic state seemed to be the state approximating this condition best. Average endocardial and epicardial radii were computed for each cross-section. From these radii, from the axial coordinate z corresponding to each cross-section and from descriptions of the anatomical structure of the heart, the geometry shown in Fig. 2 is derived. The geometry is subdivided in thirty eight-node finite elements. The upper elements (10, 11, 12) represent the annulus fibrosus and are elements with a circumferential fibre orientation.

Several authors (Hort, 1960; Streeter and Hanna, 1973; Ross and Streeter, 1975) have measured changing fibre orientations across the myocardial wall. Therefore, all the elements which do not belong to the annulus fibrosus have a fibre orientation which depends quadratically on the isoparametric coordinate ξ (Fig. 2). Stresses are computed in each integration point of the element using the local fibre orientation following from the given quadratic relationship. The fibre direction is always chosen parallel to the plane β–β which is tangential to the circumferential direction and the isoparametric coordinate η. The result is that at the endocardial surface the fibre direction is tangential to the endocardium, and at the epicardial surface, is tangential to the epicardium. The unit vector $\mathbf{B}_1$ of the local orthonormal basis $(\mathbf{B}_1, \mathbf{B}_2, \mathbf{B}_3)$ is chosen perpendicular to the plane β–β. The unit vector $\mathbf{B}_3$ (i.e. the fibre direction) encloses an angle Ψ with the base vector $\mathbf{g}_\theta$ (i.e. the circumferential direction) of the global coordinate system (r, z, θ). The transmural variation of the angle Ψ is chosen according to experimental data of Streeter and Hanna (1973). The transmural change in fibre orientation is steeper at the apex than at the equator (Fig. 3).

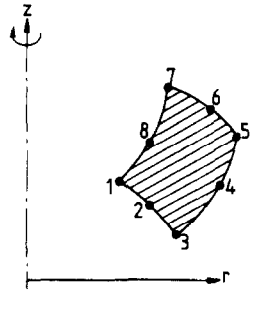

Fig. 1. Cross-section of a rotationally symmetric eight-node isoparametric ring-shaped element of the Serendipity family (Zienkiewicz, 1977, p. 157) as used in the present study.

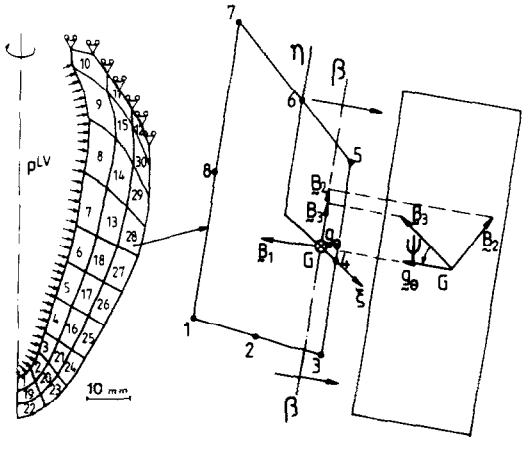

Fig. 2. The finite element mesh for the deformation model, close-up of element 28 and projection of the plane β–β at integration point G. The variables ξ and η are the isoparametric coordinates of the element. The plane β–β is perpendicular to the plane of the finite element mesh and tangent to the curve ξ = constant. The local orthonormal basis $(\mathbf{B}_1, \mathbf{B}_2, \mathbf{B}_3)$ is chosen such that the vector $\mathbf{B}_1$ is perpendicular to the plane β–β and $\mathbf{B}_3$ defines the local fibre direction. The fibre angle Ψ encloses the vector $\mathbf{B}_3$ and the circumferential direction $(\mathbf{g}_\theta)$. The constitutive law described in the appendix is defined with respect to the orthonormal basis $(\mathbf{B}_1, \mathbf{B}_2, \mathbf{B}_3)$.

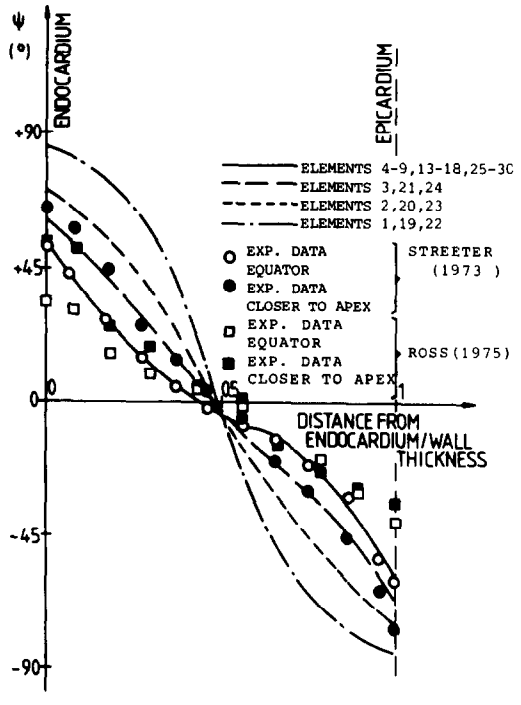

Fig. 3. Transmural distribution of the fibre angle Ψ in the model. This distribution is chosen on the basis of experimental data of Streeter and Hanna (1973) and Ross and Streeter (1975).

In order to compare the model results with experimental data on distributions of sarcomere length, we need to choose the initial sarcomere lengths in the model. For reasons of simplicity, we assume a homogeneous distribution of sarcomere length. Following Spotnitz *et al.* (1966), Pollack and Krueger (1976), Krueger and Pollack (1975), Grimm *et al.* (1980), Van Heuningen *et al.* (1982), we choose the initial sarcomere length:

$$L^s = 1.9\ \mu\text{m}. \tag{12}$$

At the upper edge of the annulus fibrosus, only radial displacement is allowed. The intramyocardial pressure at the nodes of the epicardium are set equal to the pressure in the venous epicardial vessels, thus neglecting any significant pressure drop across the venous vessel walls. However we should keep in mind that this choice can be questioned. Other degrees of freedom are not prescribed. So, at the endocardial surface the intramyocardial pressure is free. No blood is allowed to cross the endocardial surface. At the endocardial side of elements 1–9 a uniform intraventricular pressure p^{LV} is applied as an external load. The loads exerted by the papillary muscles and by the pericardium are neglected.

MATERIAL PROPERTIES

The initial coronary blood volume fraction N^f is the blood volume fraction at zero perfusion pressure and in the absence of all external loads. Klein (1945), Gibson *et al.* (1946), Salisbury *et al.* (1961), Crystal *et al.* (1981) and Eliasen *et al.* (1982) measured values ranging from 4.8 ml (100 g)$^{-1}$ LV to 8.4 ml (100 g)$^{-1}$ LV on excised hearts (Spaan, 1985). Extrapolation of the results of Morgenstern *et al.* (1973) to zero coronary perfusion pressure leads to 6 ml (100 g)$^{-1}$ LV. As an average we choose:

$$N^f = 0.06. \tag{13}$$

The permeability tensor ${}^{\circ}\underline{K}$ is defined with respect to a local orthonormal basis ($\mathbf{B}'_1$, $\mathbf{B}'_2$) (Fig. 4):

$${}^{\circ}\underline{K} = {}^{\circ}K_{ij}\,\mathbf{B}'_i\mathbf{B}'_j \quad (i,j=1,2). \tag{14}$$

As the larger vessels run mainly in the transmural direction ($\mathbf{B}'_1$ direction) we arbitrarily choose:

$${}^{\circ}K_{11} = 4\,{}^{\circ}K_{22} \tag{15}$$

$${}^{\circ}K_{12} = 0. \tag{16}$$

The value of ${}^{\circ}K_{11}$ will be evaluated by choosing the consolidation time of the two-phase model to be of the same order of magnitude as the time constant associated with emptying of the intramyocardial coronary vascular compartment. The latter is found in the order of 3 s as evaluated by Spaan *et al.* (1981) from measurements carried out at an initial perfusion pressure of about 14 kPa. As emptying of the intramyocardial coronary vascular compartment is associated with volume rather than shape change of the tissue, we assume the tissue to be elastic. Assuming the consolidation to be roughly one-dimensional and linear, we can evaluate the consolidation time t^{linear} of the left ventricular wall by [Lambe and Whitman, 1979, p. 410, equation (27.12)]:

$$t^{\text{linear}} = \frac{h_0^2}{c^c K_{11}} \tag{17}$$

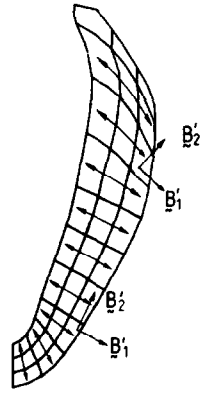

Fig. 4. Preferential direction of the largest intramyocardial vessels. The arrows represent the assumed preferential direction of these vessels. The unit vector $\mathbf{B}'_1$ is chosen parallel to this direction, the unit vector $\mathbf{B}'_2$ is perpendicular to this direction.

where h_0 is the wall thickness, with

c^c = the volumetric modulus

K_{11} = the permeability in the $\mathbf{B}'_1$ directions at 14 kPa perfusion pressure.

Equation (17) assumes that the permeability is constant during the consolidation. In reality the permeability of the medium should drop as more fluid is leaving the pores. Computations including this non-linear effect show that the consolidation takes roughly twice as long in the non-linear case than in the linear case (Huyghe, 1986). Therefore, we write:

$$t^{\text{non-lin}} = \frac{2 h_0^2}{c^c K_{11}}. \tag{18}$$

For $t^{\text{non-lin}} = 3$ s (Spaan *et al.*, 1981), the wall thickness $h_0 = 12$ mm and the volumetric modulus $c^c = 10$ kPa (Huyghe, 1986), we calculate:

$$K_{11} = 9.6 \frac{\text{mm}^2}{\text{kPa s}}. \tag{19}$$

Assuming that coronary blood volume varies by 0.5 ml (100 g)$^{-1}$ LV per kPa arterial pressure change (Morgenstern *et al.*, 1973), we find that:

$$n^f = N^f + 0.07 \tag{20}$$

with

n^f = coronary blood volume fraction at 14 kPa perfusion pressure

N^f = coronary blood volume fraction at zero perfusion pressure.

Using equation (10), we find for $N^f = 0.06$:

$${}^{\circ}K_{11} = \left(\frac{N^f}{n^f}\right)^2 K_{11} \cong 2 \frac{\text{mm}^2}{\text{kPa s}}. \tag{21}$$

It is clear that none of these quantifications is more than a rough estimate of the order of magnitude of the parameter. A detailed quantification of the coronary vascular geometry is a possible way of evaluating the above parameters with greater accuracy.

The material law which we adopted is the quasi-linear viscoelastic model of the material as described in Huyghe *et al.* (1991) and shortly reviewed in the Appendix. The reason for choosing for quasi-linearity of the viscoelastic law was mainly numerical. Using the superposition principle we avoid the need to keep the complete history of deformation in memory.

NUMERICAL SIMULATIONS

Parameter variation

In order to gain insight into the influence of the variation of different parameters on the passive behaviour of the left ventricular wall, parameter variations are carried out relative to a reference choice of parameters (Table 1). The parameter values describe an elastic material, as both relaxation parameters d and Σ^0 are set to zero. The values of c^c, c^n, a^f, a^{cf} and a^b are chosen on the basis of experimental data of stress–strain relationships of myocardial tissue from the literature (Huyghe *et al.*, 1991). The cross fibre stiffness a^{cf} is assumed to shift from 10 at the apical endocardium to 21 at the base (Fig. 5). Due to lack of experimental data on shear behaviour, the values of c^s and a^s are arbitrarily chosen. For the annulus fibrosus (elements 10, 11 and 12 of Fig. 2) we choose different values for c^n, a^{cf} and N^f:

$$c^n = 0.02\,\text{kPa};\ a^{cf} = 18;\ N^f = 0.01. \tag{22}$$

The value of N^f for the annulus is expected to be lower than for the rest of the model because a fibrous structure usually contains less blood than muscle does. As no data are available on anisotropy of the annulus, we choose a^{cf} equal to a^f. Finally, as we expect the collagenous structure to be stiffer than muscle tissue, we increase the value of c^n.

The Crank–Nicholson constant is set to 0.5. Before applying any intraventricular pressure, the intramyocardial coronary blood volume is increased from

Table 1. Reference choice of parameters

Symbol	Value	Unit
a^b	12	—
a^{cf}	10 → 21 (A → B, Fig. 5)	—
a^f	18	—
a^s	15	—
c^c	10	kPa
c^n	0.01	kPa
c^s	10	kPa
d	0	—
${}^{\circ}K_{11}$	2	mm^2 kPa^{-1} s^{-1}
${}^{\circ}K_{22}$	0.5	mm^2 kPa^{-1} s^{-1}
N^f	0.06	—
Σ^0	0	s^{-1}

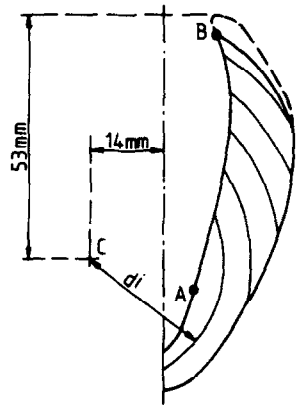

Fig. 5. The cross-fibre stiffness a^{cf} is computed according to the distance d^i between the integration and the point C. It is a linear function of d^i and takes the value 10 at point A and the value 21 at point B.

Table 2. Sensitivity of pressure–volume relations to changes in various parameters

Input	$\frac{V^{LV} \text{ at } p^{LV} = 1 \text{ kPa}}{V^{LV} \text{ at } p^{LV} = 0 \text{ kPa}}$	$\frac{V^{LV} \text{ at } p^{LV} = 2 \text{ kPa}}{V^{LV} \text{ at } p^{LV} = 0 \text{ kPa}}$
Reference choice of parameters	1.26	1.52
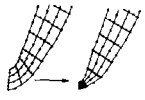		
Narrow apex	1.28	1.53
Properties of annulus = properties of wall	1.26	1.52
Incompressibility: ${}^{\circ}K_{11} = {}^{\circ}K_{22} = 0$	1.25	1.49
Decreased compressibility: $c^{c} = 50$ kPa	1.25	1.50
Homogeneous cross-fibre stiffness: $a^{cf} = 10$	1.30	1.54
Homogeneous cross-fibre stiffness and inhomogeneous fibre stiffness: $a^{cf} = 10$, $a^{f} = 18 \rightarrow 9$ (A → B, Fig. 5)	1.32	1.57
Reduced biaxial stiffness: $a^{b} = 0$	1.43	1.79
Decreased initial normal stiffness: $c^{n} = 0.002$ kPa	1.56	1.87
Increased initial shear stiffness: $c^{s} = 50$ kPa	1.20	1.40
Decreased initial shear stiffness: $c^{s} = 2$ kPa	1.32	1.55
$c^{s} = 0.4$ kPa	1.34	1.55

$N^{f} = 0.06$ to $n^{f} = 0.115$. This increase simulates the added coronary volume following application of the coronary perfusion pressure. According to Morgenstern *et al.* (1973) the increase of coronary volume of 5.5% of the total myocardial volume corresponds to a perfusion pressure of 11 kPa. Subsequently, the intraventricular pressure is increased from 0 to 3 kPa at a rate of 0.15 kPa s^{-1}. During this loading procedure, the intramyocardial pressure at the epicardial nodes is kept constant, thus allowing exchange of blood between the intramyocardial coronary bed and the epicardial vessels.

After using this procedure with the above choice of parameter values, the same procedure is repeated 11 times when changing one of the parameters at a time and keeping all other parameters at their reference value. The resulting relative cavity volume changes are listed in Table 2. The shape of the apex, the stiffness of the annulus fibrosus, the compressibility and the inhomogeneous cross fibre stiffness do not affect the pressure–volume relationship significantly. As no data are available on shear behaviour of isolated heart muscle specimens, special attention is paid to the way shear parameters affect the passive ventricle. This influence can be understood best by comparing the transmural distribution of sarcomere length at different values of the shear parameters (Fig. 6). Changes in the value of c^{s} affect the sarcomere length of the mid-layers more than the subendocardial and subepicardial sarcomere length. Since the mid-layer fibres are oriented circumferentially and the subendocardial and subepicardial fibres are oriented in a more axial direction, we can infer from Fig. 6 that at low values of c^{s} the ventricle expands more radially. The torsion of the ventricular model was found to increase with decreasing shear stiffness. In all cases, however, the rotation of the apex about the axis of symmetry

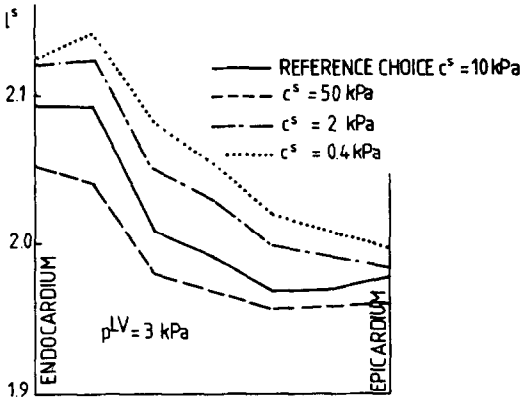

Fig. 6. Simulation of transmural distribution of sarcomere length at the equator of the elastic left ventricle during passive loading for different values of the shear parameter c^{s}. Left ventricular pressure is 3 kPa.

remained lower than 0.1 rad. During loading, the rotation of the apex was in a clockwise direction for an observer looking from apex to base.

After loading the left ventricular model from $p^{LV} = 0$ kPa to $p^{LV} = 3$ kPa, unloading of the model can also be performed. It was found that for the elastic left ventricle, the pressure–volume relationship during unloading was indistinguishable from that during loading. This result shows that the energy dissipated by the viscosity of the coronary blood volume is negligible during passive loading.

Quasi-linear viscoelasticity

Once quasi-linear viscoelasticity of the wall material is introduced into the model, the results are found to be quite different. In order to illustrate the effect of viscous dissipation clearly we chose a high value of viscosity ($d = 10$). Figure 7 shows left ventricular press-

ure vs relative volume change during loading and unloading of the passive viscoelastic left ventricle. At a low loading rate (solid line) we see that the loading curve is different from the unloading curve. As the cycle of loading and unloading is repeated, the model tends towards a closed hysteresis starting at a higher zero-pressure volume than the original zero-pressure volume. The shape of the transmural sarcomere length distribution generated during loading is partly maintained after unloading (Fig. 8). During this procedure, the model is intermittently subjected to faster load changes (Fig. 7, dashed lines). During these fast loadings, we see that the left ventricular model behaves in a stiffer way. After the simulation, residual stresses of up to 1 kPa are found in the ventricular wall model. These stresses are predominantly compressive in the inner half of the wall and predominantly tensile in the outer half of the wall.

Intramyocardial blood volume

In the previous computations, the intramyocardial blood volume was raised from its initial value $N^f = 0.06$ to the value $n^f = 0.115$ prior to raising the intraventricular pressure. The first loading curve of the viscoelastic computation, illustrated in Fig. 7, is now recomputed twice: once after raising the coronary volume from $N^f = 0.06$ to $n^f = 0.09$, and once after raising the coronary volume from $N^f = 0.06$ to $n^f = 0.14$. The resulting pressure–volume curve shifts to the left with increasing coronary blood volume (Fig. 9). The effect of coronary vascular volume on the stiffness of the ventricular model is greater at larger ventricular volumes. At a cavity volume equal to 160% of the initial, stress-free cavity volume, left ventricular pressure increases from 1.5 to 2.0 kPa when raising the intracoronary blood volume from 9 to 14 ml $(100\ g)^{-1}$ left ventricle.

Final simulation

On the basis of the computations mentioned so far, the choice of parameter values was adapted as shown in Table 3 except that for the annulus fibrosus the values of (22) remain valid, and that for the apical elements (elements 1, 19 and 22 of Fig. 2) the values of c^n and c^s are amended:

$$c^s = 1\,\text{kPa}, \qquad c^n = 0.1\,\text{kPa}. \tag{23}$$

Without this stiffening of the apex, the model was unstable in this region. This instability is probably related to the proximity of the symmetry axis. If, in addition, we choose an initial sarcomere length of 1.9 μm endocardially, 2.0 μm epicardially, and with linearly interpolated values within the wall, we find sarcomere length distributions during passive loading and unloading as shown in Fig. 10.

DISCUSSION

The present study shows that (1) torsion can be included into a large deformation axisymmetric finite element model of the left ventricle; (2) residual stresses

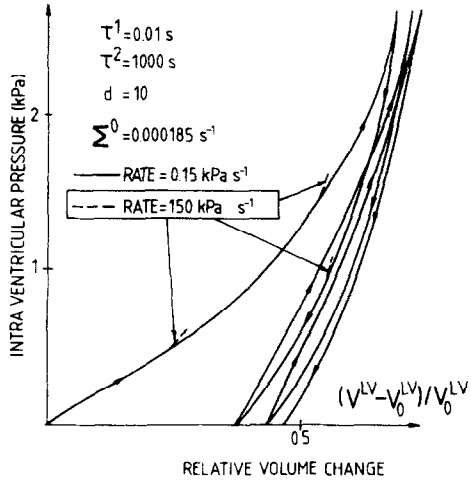

Fig. 7. Simulated pressure–volume relationship of the viscoelastic passive left ventricle at different rates of pressure change. At three sites a departure is shown at a tenfold rate.

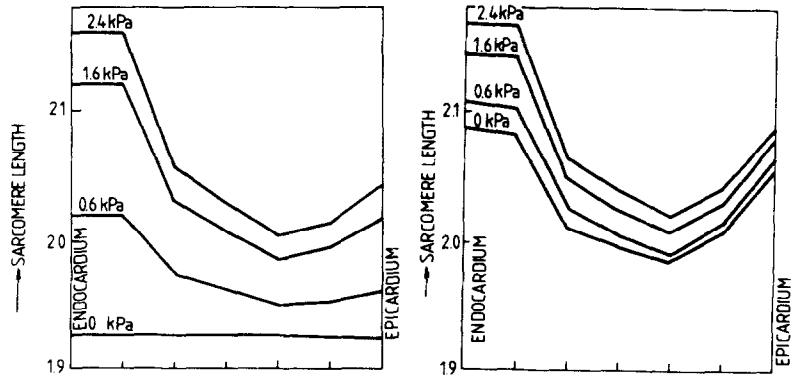

Fig. 8. Transmural distribution of sarcomere length at the equator as predicted by the model. The left panel shows results of the first loading curve shown by Fig. 7, and the right panel of the third and last loading curve.

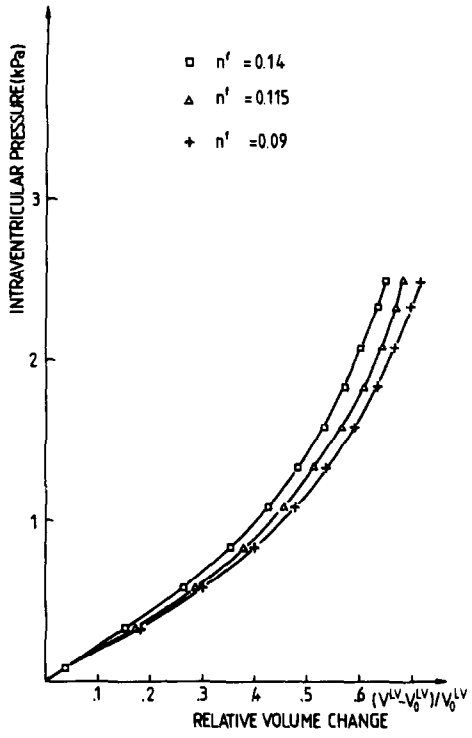

Fig. 9. Simulated pressure–volume relations of the passive left ventricle at different levels of intramyocardial blood volume. The ventricular wall stiffens at increased intramyocardial blood volume. The initial and current intracavitary volume of the left ventricular model are V_0^{LV} and V^{LV} respectively.

Table 3. Adapted choice of parameter values

Symbol	Value	Unit
a^b	12	—
a^{cf}	10	—
a^f	18	—
a^s	15	—
c^c	10	kPa
c^n	0.008	kPa
c^s	0.1	kPa
d	0.1	—
$^oK_{11}$	2	$mm^2\,kPa^{-1}\,s^{-1}$
$^oK_{22}$	0.5	$mm^2\,kPa^{-1}\,s^{-1}$
N^f	0.06	—
Σ^0	0.000185	s^{-1}
τ^1	0.01	s
τ^2	1000	s

in the ventricular wall can be explained as a consequence of viscoelasticity; (3) quasi-linear viscoelasticity is able to reflect only partially the viscoelastic properties of the left ventricular myocardium; and (4) a two-phase finite element model is able to simulate changes of ventricular properties following changes of intracoronary blood volume.

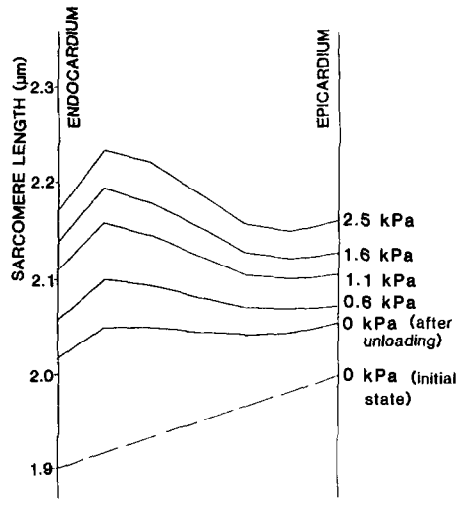

Fig. 10. Simulation of transmural equatorial sarcomere length distributions during passive loading using the adapted set of parameter values of Table 3.

Geometry and boundary conditions

We assume that the myocardial wall is stress-free at the start of the simulation. Even in a myocardial wall without external load, significant stress (= pre-stress) is present (Omens and Fung, 1990). This is evidenced by the opening angles seen when the heart is slit open. The choice of a stress-free ventricle at the start of the simulation, though apparently conflicting with this observation, does not prevent the ventricle to exhibit the property of 'pre-stress' in the unloaded state after a simulation including viscoelasticity. In fact, the computed residual stresses after the viscoelastic simulation are consistent with the observation of Omens and Fung, and suggest that viscoelasticity may be an underlying mechanism causing residual stresses in the heart wall. The compressive residual stresses in the inner half of the wall lead to a reduction of concentration of tensile stress in the subendocardial region during passive loading.

Parameter variation

The results shown in Table 1 indicate that the geometry of the apex, local inhomogeneities, the compressibility and the permeability do not appear to play a major role in the passive pressure–volume relationships of the model. However, the non-linearity of the model calls for careful interpretation of the results. After all, the influence of one parameter on the pressure–volume relationship might depend on the other parameter values. Comparison of Fig. 6 with measured sarcomere length distributions (Fig. 11), reveals that the elastic model is too stiff. Decreasing the value of the normal stiffness would lead to an overall reduction of the stiffness of the model. However, this choice is not in accordance with the ex-

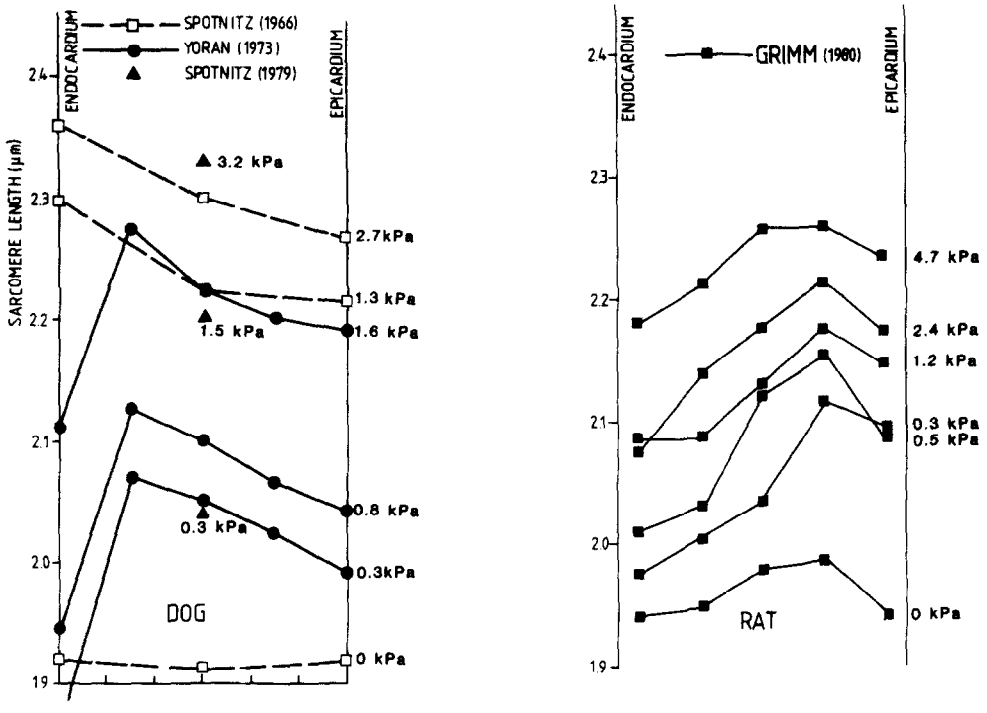

Fig. 11. Transmural distribution of sarcomere length in passively filled canine (left pannel) and rat (right pannel) left ventricles as measured by various investigators.

periments on normal stiffness of isolated myocardial tissue specimens available in the literature (Van Heuningen *et al.*, 1982). The overestimation of ventricular stiffness can more readily be counteracted by choosing a low shear stiffness, suggesting that a low shear stiffness is more realistic than a high shear stiffness. Studies based on histological data (Caulfield and Borg, 1979; Horowitz *et al.*, 1988) point in the same direction of a low shear stiffness.

Quasi-linear viscoelasticity

Considering the inability of quasi-linear viscoelasticity to adequately describe the stress–strain–time relationships of isolated myocardial specimens (Huyghe *et al.*, 1991), one could wonder why quasi-linear viscoelasticity was used in this finite element formulation. Quasi-linearity allows the saving of large amounts of memory bits during the computation. Whereas non-quasi-linear viscoelasticity requires the storage of all previous states of deformations throughout the incremental time integration, quasi-linearity allows the use of a recursive scheme requiring the storage of only one viscous stress tensor per Maxwell element and per integration point. This significant numerical advantage is the main reason for choosing for quasi-linearity. Rankin *et al.* (1977) found that the diastolic stiffness of canine left ventricles depends upon the stretch rate at which they are loaded. Figure 7 shows that quasi-linear viscoelasticity describes a stretch rate dependency of the ventricular stiffness. However, Rankin *et al.* (1977) also found that the static pressure–volume curve is not significantly affected by a pressure overload of 15 min produced by inflating implanted aortic occluders in five dogs. Therefore, the shift of the zero-pressure volume during repeated passive pressure loading of the quasi-linear viscoelastic model (Fig. 7) does not seem to be consistent with the experiment of Rankin *et al.* (1977). This comparison of model and experiments shows that quasi-linear viscoelasticity is able to reflect only partially the diastolic properties of myocardial tissue. The right panel of Fig. 8 illustrates that after a few loading–unloading cycles the shape of the transmural sarcomere length distribution is similar for different levels of the intraventricular pressure. The same phenomenon is seen in Fig. 10. This similarity of shape does not hold for the elastic ventricular model (Fig. 6). Variations in pre-load result in a more uniform variation of sarcomere length of the viscoelastic model than of the elastic model. Thus, the diastolic viscoelasticity of the ventricular model levels off transmural differences of pre-load-induced sarcomere stretch. The experimentally measured transmural sarcomere length distributions (Fig. 11) are more in favour of similarity of shape of the sarcomere length distribution at different pre-loads than of dissimilarity.

Intramyocardial blood volume

Figure 10 shows that the model is able to simulate the dependence of the ventricular compliance on the intracoronary blood volume as experimentally measured by Olsen *et al.* (1981) and Vogel *et al.* (1982). On

the basis of the experimental quantification of the relationship of coronary perfusion pressure and intracoronary blood volume by Morgenstern *et al.* (1973), we infer that the three values of intracoronary blood volume chosen in Fig. 10 correspond to coronary perfusion pressures of 6, 11 and 14 kPa. This implies that the model predicts that at constant cavity volume, the left ventricular pressure increases from 1.5 to 2.0 kPa when raising the perfusion pressure from 6 to 14 kPa. The same shift of coronary perfusion pressure causes an increase in left ventricular pressure from 1.5 to 2.4 kPa in potassium arrested hearts according to the experimental data of Olsen *et al.* (1981), while Vogel *et al.* (1982) found an increase of left ventricular pressure from 1 to 1.3 kPa and from 3 to 3.8 kPa in intact hearts, indicating that model results are within the range of experimentally measured values. Vogel *et al.* (1982) conclude from their experiments that it seems likely that the direct determinant of the effect of coronary perfusion on diastolic ventricular compliance is coronary vascular volume. The present model contains a mechanism whereby an increase in coronary vascular volume results in an overall increase in strain in the myocardial model. This increase in strain in turn results in an increase in stiffness because of the exponential elastic response of the quasi-linear viscoelastic law.

Final simulation

On the basis of the above computations, the choice of parameter values is adapted. The choice of parameters is such that conflict with experimental data on isolated muscle specimens is avoided, and the resulting properties of the ventricular model are consistent with experimental data. However, the small number of experimental data, the variety of conditions under which they are obtained, and the difficulties encountered by the investigators to precisely define these conditions, forced us to use our own discretion for some of the choices. The model results shown in Fig. 10 are fairly consistent with the experimental data shown in Fig. 11. However, we should keep in mind that both two-phase behaviour and viscoelasticity are time-dependent phenomena. Therefore, any distribution of sarcomere length depends to some extent on the previous history of the ventricle. The history of each of the ventricles used during the experiments referred to in Fig. 11 is mainly a succession of systolic contraction and diastolic relaxation. In order to be able to compare model results and experiment quantitatively, the model should be subjected to the same type of history before comparing the diastolic data of model and experiment.

Poroelasticity vs viscoelasticity

In the finite element model, two different types of time-dependent phenomena are included: redistributions of coronary blood in the wall and viscoelasticity of myocardial tissue. Including only one of the two time-dependent phenomena did not allow a description of all of the experimentally observed facts satisfactorily. Viscoelasticity alone is unable to explain changes in myocardial volume following a change in perfusion pressure as measured by Morgenstern *et al.* (1973). Poroelasticity alone, on the other hand, does not lead to a significant difference between dynamic and static diastolic stiffness of the model, nor to residual stresses in the wall, nor is it able to explain the hysteresis loops observed in stress–strain relationships of isolated myocardial specimens. Hence, it seems necessary to consider the myocardial tissue to be poroviscoelastic.

Acknowledgements—The authors gratefully acknowledge the contribution of Dr H. J. Grootenboer (Twente University) and of L. Blankenvoort to the finite element implementation; the advice of Dr F. Veldpaus (Eindhoven University of Technology) on tensor analysis; and the many discussions with Dr C. Oomens (Eindhoven University of Technology).

REFERENCES

Arts, T. (1978) A mathematical model of the dynamics of the left ventricle and the coronary circulation. Ph.D. thesis, University of Limburg, Maastricht, The Netherlands.

Arts, T., Veenstra, P. C. and Reneman, R. S. (1982) Epicardial deformation and left ventricular wall mechanics during ejection in the dog. *Am. J. Physiol.* **243,** H379–H390.

Biot, M. A. (1972) Theory of finite deformation of porous solids. *Indiana Univ. Math. J.* **21,** 597–620.

Bowen, R. M. (1976) Theory of mixture. In *Continuum Physics* (Edited by Eringen, A. C.), Vol. 3, pp. 1–127. Academic Press, New York.

Bowen, R. M. (1980) Incompressible porous media by use of the theory of mixtures. *Int. J. Engng Sci.* **18,** 1129–1148.

Caulfield, J. B. and Borg, T. K. (1979) The collagen network of the heart. *Lab. Invest.* **40,** 364–372.

Crystal, G. J., Downey, H. F. and Bashour, F. A. (1981) Small vessel and total coronary blood volume during intracoronary adenosine. *Am. J. Physiol.* **241,** H194–H201.

Eliasen, P., Amtorp, O., Tondevold, E. and Haunso, S. (1982) Regional blood flow, microvascular blood content and tissue hematocrit in canine myocardium. *Cardiovasc. Res.* **16,** 593–598.

Fung, Y. C. (1981) *Biomechanics: Mechanical Properties of Living Tissues.* Springer, New York.

Gibson, J. G. II, Seligman, A. M., Peacock, W. C., Aub, J. C., Fine, J. and Evans, R. C. (1946) The distribution of red cells and plasma in large and minute vessels of the normal dog determined by radioactive isotopes of iron and iodine. *J. Clin. Invest.* **25,** 848–857.

Grimm, A. F., Lin, H. L. and Grimm, B. R. (1980) Left ventricular free wall and intraventricular pressure–sarcomere length distributions. *Am. J. Physiol.* **239,** H101–H107.

Horowitz, A., Sheinman, I. and Lanir, Y. (1988) Non-linear incompressible finite element for simulating loading of cardiac tissue—Part II: three dimensional formulation for thick ventricular wall segments. *ASME J. biomech. Engng* **110,** 62–68.

Hort, W. (1960) Makroscopische und micrometrische Untersuchungen am Myocard verschieden stark gefullter linker Kammern. *Virchows Arch.* (Pathol. Anat.) **333,** 523–564.

Huyghe, J. M. (1986) Non-linear finite element models of the beating left ventricle and the intramyocardial cornary circulation. Ph.D. thesis, Eindhoven University of Technolgy, Eindhoven, The Netherlands.

Huyghe, J. M., Campen, D. H. van, Arts, T. and Heethaar, R. M. (1991) The constitutive behaviour of passive heart muscle tissue: a quasi-linear viscoelastic formulation. *J. Biomechanics* (in press).

Klein, J. R. (1945) Estimation of blood in tissue. *Arch. Biochem.* **8,** 421–424.

Krueger, J. W. and Pollack, G. H. (1975) Myocardial sarcomere dynamics during isometric contraction. *J. Physiol.* **251,** 627–643.

Kwan, M. K., Lai, W. M. and Mow, V. C. (1990) A finite deformation theory for cartilage and other soft hydrated connective tissues—I. Equilibrium results. *J. Biomechanics* **23,** 145–155.

Lambe, T. W. and Whitman, R. V. (1979) *Soil Mechanics.* Wiley, Chichester.

Meijer, K. L. (1985) *Computation of stresses and strains in saturated soil.* Ph.D. thesis, Delft University of Technology, Delft, The Netherlands.

Morgenstern, C., Holtes, V., Arnold, G. and Lochner, W. (1973) The influence of coronary pressure and coronary flow on intracoronary blood volume and geometry of the left ventricle. *Pflueg. Arch.* **340,** 101–111.

Mow, V. C., Kuei, S. C., Lai, W. M. and Armstrong, C. G. (1980) Biphasic creep and stress relaxation of articular cartilage in compression: theory and experiments. *J. biomech. Engng* **102,** 73–84.

Olsen, C. O., Attarian, D. E., Jones, R. N., Hill, R. C., Sink, J. D., Lee, K. L. and Wechsler, A. S. (1981) The coronary pressure–flow determinants of left ventricular compliance in dogs. *Circ. Res.* **49,** 856–865.

Omens, J. H. and Fung, Y. C. (1990) Residual strain in rat left ventricle. *Circ. Res.* **66,** 37–45.

Oomens, C. W. J., Campen, D. H. van and Grootenboer, H. J. (1987) A mixture approach to the mechanics of skin. *J. Biomechanics* **20,** 877–885.

Pao, J. C. and Ritman, E. L. (1977) Viscoelastic, fibrous, finite-element, dynamic analysis of beating heart. In *Symp. Appl. Comput. Meth. Engng.*

Pollack, G. H. and Krueger, J. W. (1976) Sarcomere dynamics in intact cardiac muscle. *Eur. J. Cardiol.* **4** (suppl.), 53–65.

Rankin, J. S., Arentzen, C. E., McHale, P. A., Ling, D. and Anderson, R. W. (1977) Viscoelastic properties of the diastolic left ventricle in the conscious dog. *Circ. Res.* **41,** 37–45.

Ross, M. A. and Streeter, D. D. Jr (1975) Nonuniform subendocardial fiber orientation in the normal macaque left ventricle. *Eur. J. Cardiol.* **3,** 229–247.

Salisbury, P. F., Cross, C. E. and Riben, P. A. (1961) Physiological factors influencing coronary blood volume in isolated dog hearts. *Am. J. Physiol.* **200,** 633–636.

Simon, B. R., Wu, I. S. S., Carlton, M. W., Kazarian, L. E., France, E. P., Evans, J. H. and Zienkiewicz, O. C. (1985) Poroelastic dynamic structural models of rhesus spinal motion segments. *Spine* **10,** 494–507.

Spaan, J. A. E. (1985) Coronary diastolic pressure-flow relation and zero flow pressure explained on the basis of intramyocardial compliance. *Circ. Res.* **6,** 293–309.

Spaan, J. A. E., Breuls, N. P. W. and Laird, J. D. (1981) Diastolic; systolic coronary flow differences are caused by intramyocardial pump action in the anesthetized dog. *Circ. Res.* **49,** 584–593.

Spotnitz, H. M., Sonnenblick, E. M. and Spiro, D. (1966) Relation of ultrastructure to function in the intact heart; sarcomere structure relative to pressure volume curves of intact left ventricles of dog and cat. *Circ. Res.* **18,** 49–66.

Spotnitz, W. D., Spotnitz, H. M., Truccane, N. J., Cottrell, T. S., Gezsony, W., Malm, J. R. and Sonnenblick, E. H. (1979) Relation of ultrastructure and function; sarcomere dimensions, pressure–volume curves and geometry of the intact left ventricle of the immature canine heart. *Circ. Res.* **44,** 679–691.

Streeter, D. D. Jr and Hanna, W. T. (1973) Engineering mechanics of successive states in canine left ventricular myocardium: II. Fiber angle and sarcomere length. *Circ. Res.* **33,** 657–664.

Terzaghi, K. (1943) *Theoretical Soil Mechanics.* Wiley, New York.

Van Heuningen, R., Rijnsburger, W. H. and Keurs, H. E. D. J. ter (1982) Sarcomere length control in striated muscle. *Am. J. Physiol.* **242,** H411–H420.

Vogel, W. M., Apstein, C. S., Griggs, L. L., Gaasch, L. and Ahn, J. (1982) Acute alterations in left ventricular diastolic chamber stiffness: role of the erectile effect of coronary arterial pressure and flow in normal and damaged hearts. *Circ. Res.* **51,** 465–478.

Yoran, C., Covell, J. W. and Ross, J. Jr (1973) Structural basis for the ascending limb of left ventricular function. *Circ. Res.* **32,** 297–303.

Zienkiewicz, O. C. (1977) *The Finite Element Method,* 3rd Edn. McGraw-Hill, New York.

APPENDIX

The viscoelastic law used for the passive behaviour of the solid is described with respect to a local orthonormal basis ($\mathbf{B}_1$, $\mathbf{B}_2$, $\mathbf{B}_3$) (Fig. 2). The unit vector $\mathbf{B}_1$ is perpendicular to the myocardial wall. The unit vector $\mathbf{B}_3$ is parallel to the fibre direction and encloses an angle Ψ with the circumferential direction. The second Piola–Kirchhoff effective stress is split into two parts, one resulting from volume change of the myocardial tissue (S^c_{ij}), the other resulting from shape change of the myocardial tissue (S^s_{ij}):

$$S_{ij} = S^c_{ij}(E_{kl}) + S^s_{ij}(E_{kl}, t) \tag{A.1}$$

in which E_{ij} represents the Green strain components with respect to the local orthonormal basis ($\mathbf{B}_1$, $\mathbf{B}_2$, $\mathbf{B}_3$). S_{ij} is related to the Cauchy effective stress $\underline{s}$ according to:

$$S_{ij} = J\,\mathbf{B}_i \cdot \underline{F}^{-1} \cdot \underline{s} \cdot \underline{F}^{-\mathrm{C}} \cdot \mathbf{B}_j. \tag{A.2}$$

As volume change does not induce shear strain, and viscous effects are associated with shear rate, we assume that the stress S^c_{ij} is elastic. The strain E_{ij} is zero for the reference state of the finite element mesh depicted in Fig. 2, which corresponds to 0 kPa left ventricular pressure. The elastic stress $\underline{S}^c$ is derived from the isotropic strain energy function C:

$$S^c_{ij} = \frac{\partial C}{\partial E_{ij}}. \tag{A.3}$$

We assume that S^c_{ij} is linearly related to volume change.

$$C = \frac{c^c}{2}(J-1)^2 \tag{A.4}$$

with

J = local ratio of current and initial myocardial volume
c^c = volumetric modulus.

The viscoelastic stress $\underline{S}^s$ obeys the quasi-linear relationship (Fung, 1981, pp. 226–253):

$$S^s_{ij}(E_{kl}, t) = \int_0^t G(t-\tau)\frac{\mathrm{d}S^e_{ij}}{\mathrm{d}\tau}(E_{kl}(\tau))\mathrm{d}\tau \tag{A.5}$$

where $G(t)$ is the reduced relaxation function:

$$G(t) = \left[1 + \int_0^\infty \Sigma(\tau)\mathrm{e}^{-t/\tau}\,\mathrm{d}\tau\right]\left[1 + \int_0^\infty \Sigma(\tau)\mathrm{d}\tau\right]^{-1} \tag{A.6}$$

and $\Sigma(\tau)$ is the relaxation spectrum:

$$\Sigma(\tau)=\frac{d}{\tau}+\Sigma^0 \quad \text{for } \tau^1<\tau<\tau^2$$

$$\Sigma(\tau)=0 \qquad \text{for } \tau<\tau^1 \text{ and } \tau>\tau^2. \tag{A.7}$$

The elastic response S^e_{ij} is specified by an orthotropic strain energy function W:

$$S^e_{ij}=\frac{1}{2}\left(\frac{\partial W}{\partial E_{ij}}+\frac{\partial W}{\partial E_{ji}}\right) \tag{A.8}$$

$$\begin{aligned}W=c^n\{&\exp(a^{cf}E_{11})-a^{cf}E_{11}+\exp(a^{cf}E_{22})\\&-a^{cf}E_{22}+\exp(a^fE_{33})-a^fE_{33}\\&+(\exp(a^bE_{11})-a^bE_{11})(\exp(a^bE_{22})-a^bE_{22})\\&+(\exp(a^bE_{11})-a^bE_{11})(\exp(a^bE_{33})-a^bE_{33})\\&+(\exp(a^bE_{22})-a^bE_{22})(\exp(a^bE_{33})-a^bE_{33})-6\}\\&+c^s\{\exp[a^s(E_{12}E_{12}+E_{13}E_{13}+E_{23}E_{23})]-1\}.\end{aligned} \tag{A.9}$$